A study of mode conversion in an oxygen–hydrogen plasma

Jay R. Johnson
Center for Space Research, Massachusetts Institute of Technology, Cambridge, Massachusetts 02139 and Geophysical Institute, University of Alaska at Fairbanks, Fairbanks, Alaska 99775-0800

Tom Chang and G. B. Crew
Center for Space Research, Massachusetts Institute of Technology, Cambridge, Massachusetts 02139

(Received 3 October 1994; accepted 7 December 1994)

Linear mode conversion is considered between the ion-cyclotron and magnetosonic branches in a multispecies plasma with parallel magnetic field gradients. The results are interpreted in terms of ion conic heating. The mode-conversion coefficients are solved using perturbation theory, a phase integral approach, and saddle-point theory. These results are compared with numerical calculations. The coefficients thus obtained demonstrate that substantial coupling occurs between the four propagating modes, and a definite absorption occurs. Such absorption corresponds to ion heating and is, under realistic circumstances, sufficient to explain the outflow and heating of ionospheric oxygen. © *1995 American Institute of Physics.*

I. INTRODUCTION

Energization of ionospheric oxygen to magnetospheric energies can be interpreted to be the result of wave absorption near the oxygen cyclotron frequency.[1–3] The mechanism by which these central plasma sheet (CPS) ions are energized seems to be well understood, but the origin and nature of the ambient turbulence remain somewhat uncertain. Because there is no obvious local source, we suggested a scenario[4] in which the waves are generated in the equatorial region of the magnetosphere and propagate along magnetic fields to lower altitudes where they heat ions. Two primary concerns about this model are (a) whether waves propagating earthward from the central plasma sheet are able to pass through a "stop gap" en route to the heating region and (b) how much wave power is available for heating ions near the oxygen gyrofrequency (about 10% of the observed wave power is required[1–3]).

To illustrate this scenario and the associated concerns, consider the low frequency dispersion relation for two ion species[5,6] as shown in Fig. 1. This dispersion relation is characterized by three separate modes which we have labeled I, II, and III. Mode I is the magnetosonic branch and is predominately right-hand circularly polarized (RHCP) at high frequency whereas mode II, which is the hydrogen ion-cyclotron branch, is predominately LHCP. Below the oxygen cyclotron frequency mode II propagates as the RHCP magnetosonic branch and mode III represents the LHCP ion-cyclotron branch. Near the crossover frequency, modes I and II couple and exchange energy.[7] Mode I also suffers a cutoff at the cutoff frequency and is separated from mode III by an evanescent region. As waves move into regions of larger magnetic field they move "down" along the dispersion curves according to the Wentzel–Kramers–Brillouin (WKB) approximation in that they satisfy the local dispersion relation. The scenario in which waves propagate earthward into a region of larger magnetic field (as is the case for waves propagating from the equatorial region to the auroral region) corresponds to waves incident from "above" the coupling-evanescent region. Some of the incident wave power is then reflected back along branches I and II, some wave power is transmitted along branches II and III "below" the heavy-ion-cyclotron frequency, and some wave power is absorbed in the evanescent region. Particle heating may result from ion-cyclotron damping of branch III (for a thermal plasma) and from the calculated absorption which typically corresponds to mode conversion to a strongly damped thermal plasma wave.

In order to address the primary concerns of our model, we consider the localized region near the oxygen gyrofrequency where the WKB approximation becomes questionable. We solve for the various transmission, reflection, and absorption coefficients both analytically and numerically and interpret the results in terms of wave energization. In order to ascertain the coefficients we employ several techniques: perturbation theory, saddle-point analysis, and phase-integral analysis. Each approach has its limitations and advantages, but they are in reasonable agreement where more than one method is applicable. We substantiate the analytical results by evaluating the coefficients numerically. Furthermore, for intermediate angle of propagation we find that two saddle points are involved in the coupling process and the linear approximation is not completely accurate. Finally, we refer the interested reader to two cataloged reports[8,9] which contain the complete details of the analytical and numerical calculations provided in this paper.

II. BASIC EQUATIONS

In the CPS the typical Alfvén wavelength far exceeds even the most energetic ion gyroradius so that a cold plasma description is reasonable. Because the mode conversion process that we consider primarily depends on magnetic field gradients, we assume a uniform density profile. At low altitudes where the heating and mode conversion processes are presumed to occur, the primary gradient in the magnetic field strength is parallel to the field. We should emphasize that perpendicular gradients are weak compared to parallel gradients for this problem so that their effects are not important in

 1070-664X/95/2(4)/1274/11/$6.00 © 1995 American Institute of Physics

Downloaded 21 Jan 2009 to 198.35.0.41. Redistribution subject to AIP license or copyright; see http://pop.aip.org/pop/copyright.jsp

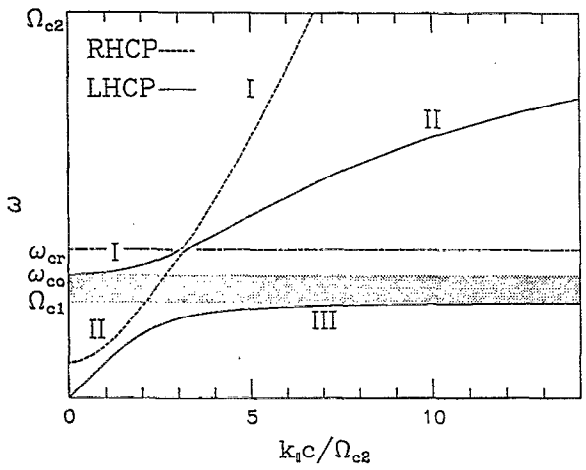

FIG. 1. Dispersion relation for a cold two-ion component plasma for nonparallel propagation. The various branches are labeled according to their predominate polarization with RHCP dashed and LHCP solid.

our calculations. Thus, our work is different from other studies in which perpendicular gradients dominate.[10–12]

With these assumptions, Maxwell's equations combined with the momentum transfer equations reduce to a set of coupled ordinary differential equations for the components of the electric field.[13] For low frequencies, the electric field parallel to the magnetic field is negligible[14] so that the equations for the circularly polarized electric field components perpendicular to the magnetic field, $E_\pm = E_x \pm iE_y$ take the compact form

$$\varepsilon^2 \Psi'' + M\Psi = 0, \tag{1}$$

where

$$M \equiv \begin{pmatrix} r - \dfrac{\kappa^2}{2} & \dfrac{\kappa^2}{2} \\ \dfrac{\kappa^2}{2} & l - \dfrac{\kappa^2}{2} \end{pmatrix}. \tag{2}$$

The two components of Ψ (ψ and ϕ) are the circularly polarized fields E_- and E_+ which are functions of the dimensionless coordinate, $z \equiv x/L_B$ where L_B is a conveniently chosen spatial scale. The characteristics of the medium are contained in the parameters: $\varepsilon \equiv 1/k_A L_B$, $\kappa \equiv k_\perp/k_A$, $k_A \equiv \omega/v_A$, $L_B \equiv B^{-1}\, dB/dz$. The rescaled Stix functions

$$\begin{matrix} r \\ l \end{matrix} = \pm \frac{\Omega_{c1}\Omega_{c2}}{\omega_{co}} \frac{(\omega \pm \omega_{co})}{(\omega \pm \Omega_{c1})(\omega \pm \Omega_{c2})}, \tag{3}$$

where v_A is the Alfvén velocity. We have taken the Fourier transform in the direction perpendicular to the magnetic field.

These equations are related to a dispersion relation which is obtained from the Fourier transform ($i\varepsilon d/dz \to n$) of the matrix equation (1),

$$n_\pm^2 = \frac{r+l}{2} - \frac{\kappa^2}{2} \pm \left[\left(\frac{r-l}{2} \right)^2 + \frac{\kappa^4}{4} \right]^{1/2}. \tag{4}$$

These equations are primarily characterized by the quantities ε, κ, and the relative spacing of the cyclotron frequencies and the cutoff. For small ε the WKB solutions most nearly approximate the correct solution in the regions where r and l are well behaved. The parameter κ characterizes the coupling between the two modes.

III. ANALYTICAL CONSIDERATIONS

A. Previous work

Mode conversion near the ion–ion crossover frequency has a rich history dating back to observations of proton whistlers.[7] It was later recognized that absorption of the compressional Alfvén wave at a deuterium gyroresonance layer could be an effective mechanism to heat fusion plasmas. A series of papers[2,15–18] specifically addressed mode conversion in an H–D plasma with parallel magnetic field gradients. Those results are applicable if the saddle point at the crossover frequency is not important as is the case for coupling at low frequencies (well below the crossover frequency) or for large angle of propagation (absorption at the ion–ion hybrid frequency). However, for small perpendicular wave vector and higher frequencies they do not retain the appropriate dispersion relation topology and only address coupling of two asymptotic modes rather than four. A more recent analysis[19] addressed this problem by retaining the coupling point associated with the crossover frequency and the four propagating plasma modes. However, that analysis does not retain coupling at both the crossover frequency and at the cutoff frequency simultaneously because their linear approximation retains only one saddle point. Moreover, the approximations made in their analysis limit its applicability for nonparallel wave propagation to small ion densities (less than 3%). In this section we calculate the coefficients using several different methods (several of the methods have been applied to a H–D plasma[15–18]). Where applicable, the saddle-point method is best as it allows treatment of the two coupling regions separately. We also solve the equations numerically and find that both saddle points are important for coupling—particularly for intermediate angles of propagation.

B. Saddle-point topology

Mode conversion is generally characterized by the coalescence of two propagating modes.[16,20–22] The local properties of a medium in one dimension are characterized by the dispersion relation $D(k,z)=0$. Saddle points of the dispersion relation where at least two roots coalesce occur where $\partial D/\partial k = 0$ which is satisfied for the mapping $k = k_c(z)$ which depends upon the spatial coordinate, z. At a point, z_b, the mapping, $k_c(z_b)$, becomes a double root of the dispersion relation and is referred to as a branch point. Near the saddle point, the dispersion equation may be described in terms of an embedded dispersion relation

$$D(k_c,z) + (k-k_c)^2 D_{kk}(k_c,z)/2 = 0. \tag{5}$$

Then a differential equation describing the two-mode coupling may be obtained from the Fourier transform in k so that

$$\psi''(z) + Q(z)\psi = 0 \tag{6}$$

Downloaded 21 Jan 2009 to 198.35.0.41. Redistribution subject to AIP license or copyright; see http://pop.aip.org/pop/copyright.jsp

with $Q(z)=-2D(k_c,z)/D_{kk}(k_c,z)$. By definition, the potential Q vanishes at branch points z_b where $D=0$. When coupling points are well separated, the embedded equation contains sufficient information to describe the coupling between the embedded modes. Such coupling is typically very strong if the coupling point z_b occurs close to the real axis and is weak if the coupling point is far from the real axis.

The particular dispersion relation that we are considering for low frequency waves may be obtained from the Fourier transform of Eq. (1)

$$D(k,z)=(k^2-r)(k^2-l)+\kappa^2(k^2-r+l/2), \tag{7}$$

where it is understood that r and l are explicit functions of z. The saddle points are located along contours

$$k_c(z)=0, \quad (r+l-\kappa^2)/2. \tag{8}$$

The branch points in space related to these saddle points may be obtained by solving the dispersion relation (7) along the saddle-point contours, $k_c(z)$. For the coupling point at $k_c=0$ we find the cutoff condition

$$rl=\kappa^2(r+l)/2 \tag{9}$$

which occurs at the position corresponding to the cutoff frequency

$$\omega^2=\omega_{co}^2\omega_{ii}^2\,\frac{1-\kappa^2/2}{\omega_{ii}^2-\kappa^2\omega_{co}^2/2}. \tag{10}$$

For small values of κ, this cutoff occurs at the cutoff frequency, ω_{co}, which for parallel propagation is the cutoff of the LHCP L mode. Near $\kappa^2=2$ the denominator diverges. (Actually the root approaches the lower-hybrid frequency, but our approximations, suitable for low frequencies, do not adequately describe this.) On the other hand, for $\kappa>\sqrt{2}$ a cutoff appears at low frequencies which increases as a function of κ up to the ion–ion resonance. At some critical κ the cutoff passes through the resonance.

The coupling point, $k_c=(r+l-\kappa^2)/2$, when substituted into the dispersion relation yields

$$d^2+\kappa^4/4=0, \tag{11}$$

where d is the difference function

$$d=\frac{r-l}{2}=\frac{\Omega_{c1}\Omega_{c2}}{\Omega_{co}}\,\frac{\omega(\omega^2-\omega_{cr}^2)}{(\omega^2-\Omega_{c1}^2)(\omega^2-\Omega_{c2}^2)}. \tag{12}$$

For $\kappa=0$, this condition is satisfied at the cutoff and crossover frequencies which are the zeros of the function d. As $\kappa\to\infty$, this condition is satisfied near the ion gyrofrequencies. For $\kappa\neq0$ it is clear that this condition may be satisfied only for values of complex d which correspond to the branch points, z_b, which are complex conjugate pairs. In Fig. 2 we plot values of the complex frequency along which Eq. (11) is satisfied. Equation (11) is an eighth-order equation in frequency with four complex conjugate pair solutions except at $\kappa=0$ and $\kappa\to\infty$ where the modes coalesce into a pair of real double roots. For reasonable ionospheric values of the oxygen density, the crossover frequency connects to the oxygen cyclotron frequency and the double root at $\omega=0$ connects to the heavy ion gyrofrequency. From the topology, we expect coupling to be largest when the coupling points lie near the real axis. In this sense, we see that the largest coupling takes place for small values of κ near the crossover frequency and near the $\omega=0$ root (which corresponds physically to very low altitudes), and for large values of κ the coupling occurs near the two gyrofrequencies (the other gyrofrequency at $z=16$ is not shown in Fig. 2). The topology of these branch points is discussed in detail by Le Quéau and Roux.[19]

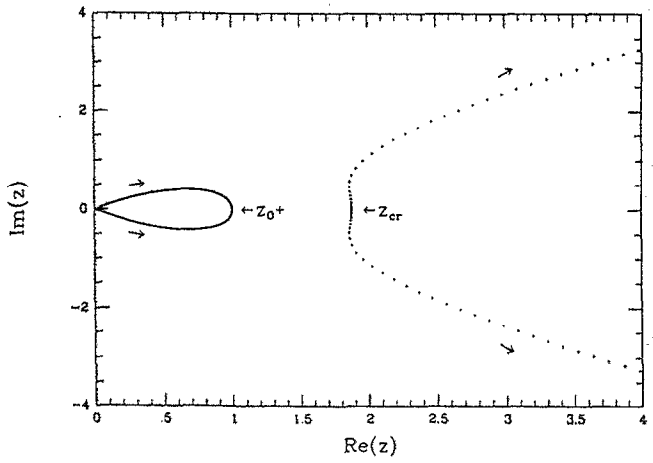

FIG. 2. The locus of solutions to Eq. (11) for varying κ. The coordinate z corresponds to the ratio ω/Ω_{c1}. The arrows indicate the direction of increasing κ.

C. Small κ—Four propagating modes

1. Perturbation and saddle-point analysis

In this section, we solve for coupling due to the saddle point at the crossover frequency. The coupling may be considered as a perturbation about parallel propagation.[4,20] Equation (1) then reduces to a hierarchy of second-order differential equations which are coupled by the known lower-order fields. The zeroth-order solutions are the two uncoupled parallel propagating R,L modes. The higher-order fields may be determined using variation of parameters. To determine the behavior of a downcoming ion-cyclotron (magnetosonic) wave, we prescribe that $E_-^{(0)}(E_+^{(0)})$ vanishes. The amplitude of the coupled wave involves an integral over a rapidly oscillating function which becomes stationary at the crossover frequency. The amplitude may be evaluated using standard methods of stationary phase.[4,23]

Comparing the Poynting flux of the incident wave above the coupling region to that of the coupled wave below the coupling region we obtain the coupling coefficient[4]

$$C\equiv\left|\frac{\hat{z}\cdot\mathbf{S}_{\text{below}}}{\hat{z}\cdot\mathbf{S}_{\text{above}}}\right|=\frac{\pi}{8\varepsilon}\,\frac{\kappa^4}{\sqrt{rd'}}\bigg|_{\omega=\omega_{cr}}\sim\frac{k_\perp^4}{k_\parallel^4}\,L_Bk_\parallel. \tag{13}$$

This result may be extended to larger values of κ if we consider the embedded dispersion relation discussed in Eq. (7). The coupling which occurs at the crossover frequency arises from the branch point which is the solution to Eq. (11), and may be described in terms of the embedded equation (6) with

Downloaded 21 Jan 2009 to 198.35.0.41. Redistribution subject to AIP license or copyright; see http://pop.aip.org/pop/copyright.jsp

$$Q(z)=\frac{1}{2}\frac{d^2+\kappa^4/4}{2s-\kappa^2}. \tag{14}$$

The function d has a zero at the crossover frequency, so that locally $d = d_{cr} + d'_{cr}\xi$ with $d_{cr}=0$. The coupling is described by the potential equation

$$\psi''(\xi)+\frac{1}{2}\frac{d'^2_{cr}\xi^2+\kappa^4/4}{2s_{cr}-\kappa^2}\psi=0, \tag{15}$$

where the sum function has been evaluated at the crossover frequency. Equation (15) then takes the form of a Weber equation. The transmission coefficient is well known[17,18,24]

$$T=\exp\left(-\frac{\pi}{8\varepsilon}\frac{\kappa^4}{d'_{cr}\sqrt{s_{cr}-\kappa^2/2}}\right). \tag{16}$$

For small values of κ, $T\approx 1-C$ as obtained in Eq. (13).

The coupling occurs as the result of finite κ and increases rapidly for small angles of propagation. For larger κ, the coupling approaches unity which means that a complete transfer of power from the predominately RHCP to the predominately LHCP mode occurs. For large magnetic field scale length $\varepsilon\to 0$ and coupling is complete so that waves propagate on their appropriate dispersion surface and do not couple to other surfaces (except for parallel propagation).

2. Phase integral analysis and tunneling

In this section we solve (1) using the phase-integral method, and interpret the results in terms of two-mode coupling for the saddle points associated with the crossover and cutoff frequencies. We show that under the condition of a large "gap" the solution is essentially a series of two-mode couplings. For a small "gap" the process is more complicated, but the coefficients still only involve the exponential factors which arise from the two-mode couplings.

To proceed, we approximate the functions r and l near the resonance

$$r\approx k_r^2, \quad l\approx k_l^2(1-a/z), \tag{17}$$

where a linearized form of the magnetic field, $B=B_0(1-z)$, has been used. The linearized function, l, retains the resonance and cutoff, while variations in the function, r, are not substantial. Near the resonance, the behavior of (1) is dominated by the singularity in l and higher-order terms in z are unimportant. If we were to include other dissipative effects, such as damping the pole would be found below the real axis.

As in standard phase-integral analysis, we continue the WKB solution around the singularity and use conservation properties to obtain the proper asymptotic form of the solution in the complex plane. From the differential equation (1) and its adjoint, we form the conserved quantity corresponding to the Poynting flux along the z axis,

$$J=i(\Psi^{\dagger\prime}\Psi-\Psi^{\dagger}\Psi') \tag{18}$$

which is conserved in space according to

$$J'=i\Psi^{\dagger}(\mathbf{M}-\mathbf{M}^{\dagger})\Psi, \tag{19}$$

where the prime denotes real derivatives along a contour with fixed imaginary part [recall that $d\psi^*/dz\neq(d\psi/dz)^*$ except along a line, $z=x+iy$, with y fixed]. The function l is singular at the heavy ion gyrofrequency so that a discontinuous jump in J occurs across the singularity.

The discontinuity from continuation above (below) the real axis is $\mp\Delta=\mp 2\pi k_l^2 a|\phi|^2_{z=0}$. Continuation above the pole corresponds to energy which is absorbed. That is $J^+<J^-$ where the superscript refers to the value along the positive (negative) real axis. Then if there is no flux in or out on the positive real axis ($J^+=0$) there is a positive energy flow from the left ($J^->0$), which is absorbed. On the other hand, if there is no flux from the left ($J^-=0$), then there is a negative flux from the right ($J^+<0$) sending wave energy, which is absorbed, into the system. The value of this energy loss clearly depends on the details of the boundary conditions. Physically, we may interpret this energy loss as resulting from resonant absorption at the gyrofrequency. Such absorption typically occurs because the cold plasma wave mode converts into a thermal wave which is readily absorbed. Conversely, if the pole lies above the real axis, a similar procedure results in an energy gain which is unphysical.

We may obtain a substantial amount of information concerning the asymptotic behavior of the solutions. The WKB solutions in this case are of the form

$$\Theta=\exp\left(\pm\frac{i}{\varepsilon}\int^z n_\pm\, ds\right). \tag{20}$$

For large values of z the indices may be expanded using the approximation (17) to give

$$n_\pm\approx n^0_\pm-\frac{k_l^2 a}{4z}\frac{\pm\delta+\sqrt{\delta^2+\kappa^4/4}}{n^0_\pm\sqrt{\delta^2+\kappa^4/4}}, \tag{21}$$

where

$$n^0_\pm=\left[\sigma-\frac{\kappa^2}{2}\pm\left(\delta^2+\frac{\kappa^4}{4}\right)^{1/2}\right]^{1/2} \tag{22}$$

with the zeroth-order sum $[\sigma=(k_r^2+k_l^2)/2]$ and difference $[\delta=(k_l^2-k_r^2)/2>0]$ functions. The four WKB solutions are

$$\begin{aligned}\Theta^{\pm}_{+}&=\exp[\pm i/\varepsilon(n_+z-\beta_+\log z/2)],\\ \Theta^{\pm}_{-}&=\exp[\pm i/\varepsilon(n_-z-\beta_-\log z/2)],\end{aligned} \tag{23}$$

where

$$\beta_\pm\equiv\frac{k_l^2 a}{2}\frac{\pm\delta+\sqrt{\delta^2+\kappa^4/4}}{n^0_\pm\sqrt{\delta^2+\kappa^4/4}} \tag{24}$$

and the coupling is characterized by the multivalued nature of the logarithm.

From these expressions we can determine the transmission coefficients for the case of incident magnetosonic waves or ion-cyclotron waves. We may extend the WKB solutions into the complex plane and use the dominance of the various solutions to determine transmission properties.[24] The solutions on the positive real axis are of the form

$$\psi=A\Theta^-_+ + B\Theta^-_- + C\Theta^+_- + D\Theta^+_+, \quad \mathrm{Arg}(z)=0, \tag{25}$$

where we have written them in order of dominance in the upper-half complex plane. The lower component, ϕ, of Ψ is

Downloaded 21 Jan 2009 to 198.35.0.41. Redistribution subject to AIP license or copyright; see http://pop.aip.org/pop/copyright.jsp

of the same form with coefficients which are related to A, B, C, and D by the dispersion relation. The WKB approximations in the complex plane, however, are at best limited to validity within certain sectors due to the Stokes phenomenon which results from the fact that the exponential solutions are too simple to adequately describe the qualitative behavior of the actual functions. Although the coefficient of the dominant solution within a given region remains unchanged, the subdominant solutions are liable to change. To accommodate this change, we make a discontinuous adjustment of the subdominant terms along the Stokes lines where the subdominant terms are least significant. The Stokes lines in this case are along the positive imaginary axis while the anti-Stokes lines are along the positive real axis. Accordingly the solution takes the general form

$$\psi = A\Theta_+^- + (B - AS_1)\Theta_-^- + (C - AS_2 - BS_3)\Theta_-^+ + (D - AS_4 - BS_5 - CS_6)\Theta_+^+, \quad \mathrm{Arg}(z) = \pi \tag{26}$$

on the negative real axis. We have added Stokes constants across the region of least dominance according to a prescription which retains the continuity of the equations in the absence of the more dominant solutions. The boundary conditions for downgoing ion-cyclotron waves are given by $A=1$, $B=S_1$, $C=D=0$ while for downgoing magnetosonic waves the boundary conditions are $A=0$, $B=1$, $C=D=0$. The leading-order coefficient for downgoing ion-cyclotron waves is

$$T_{\mathrm{IC}} = |\Theta_+^-|^2_{\mathrm{Arg}(z)=\pi} / |\Theta_+^-|^2_{\mathrm{Arg}(z)=0} = e^{-\pi\beta_+/\varepsilon}, \tag{27}$$

whereas for downgoing magnetosonic waves in the absence of an incident ion-cyclotron wave there is no transmitted flux in the ion-cyclotron mode and the transmission coefficient to the magnetosonic mode is

$$T_{\mathrm{MS}} = |\Theta_-^-|^2_{\mathrm{Arg}(z)=\pi} / |\Theta_-^-|^2_{\mathrm{Arg}(z)=0} = e^{-\pi\beta_-/\varepsilon}. \tag{28}$$

For $\kappa \ll \delta$, we find from Eq. (24) that T_{IC} is essentially the Budden coefficient for parallel propagation $[\beta_+ = k_l a(1 - O(\kappa^4))]$. With increasing κ, the tunneling diminishes. For large κ, we find that the coefficient approaches another constant, namely

$$\beta_+ = k_l^2 a / 2\sqrt{\sigma}, \tag{29}$$

which we interpret in Sec. III D 2 as Budden-like tunneling for nearly perpendicular propagation near the ion–ion hybrid frequency.

On the other hand, for the downgoing magnetosonic wave we find that for small κ Eq. (24) gives the transmission coefficient

$$T_{\mathrm{MS}} = e^{-\pi\beta_-/\varepsilon} \approx \exp\left(-\frac{\pi k_l^2 a \kappa^4}{(16\varepsilon k_r \delta^2)}\right) \approx \exp\left(\frac{\pi}{8\varepsilon}\frac{\kappa^4}{d'_{\mathrm{cr}}\sqrt{\sigma}}\right), \tag{30}$$

where $d'_{\mathrm{cr}} = 2\delta^2/k_l^2 a$. The transmission coefficient is equivalent to the coupling coefficient established in Eq. (16). For parallel propagation transmission of the magnetosonic mode is complete ($T=1$), but coupling increases rapidly with larger values of κ and transmission falls off substantially.

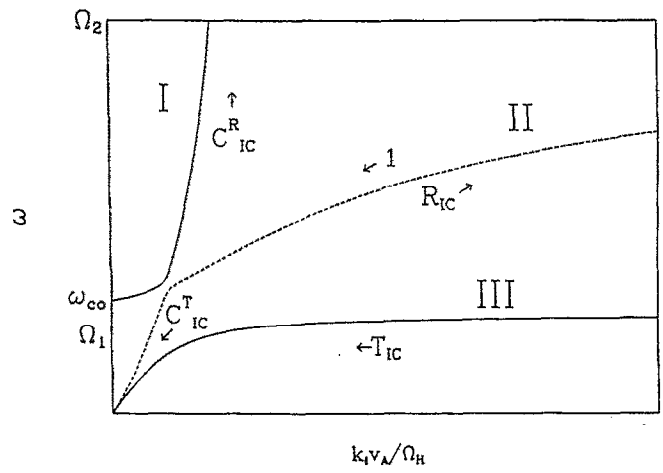

FIG. 3. Illustration of the meaning of the coefficients for a downgoing ion-cyclotron wave.

The values of the Stokes constants may not be unambiguously determined using the methods of the previous section although a number of relationships between the amplitudes of the various waves may be determined. For the case of a "large" gap, however, we may actually determine the coefficients unambiguously. In this case the WKB solution, Θ_+^-, has negligible amplitude at $-\infty$, i.e., $\beta_+ \to \infty$ so that there is no transmission in that mode. Furthermore, the restriction that no upgoing ion-cyclotron wave, Θ_+^+, be found at $-\infty$ implies that $\Delta \to 0$ so that no absorption occurs. In a detailed report[8] we have shown that in the limit of a large "gap" the transmission and reflection coefficients, defined to be the ratio of the Poynting flux of a particular wave to that of the incident wave, are

$$\begin{aligned} C_{\mathrm{IC}}^T &= 1 - e^{-\pi\beta_-/\varepsilon} = 1 - C, \\ R_{\mathrm{IC}} &= e^{-2\pi\beta_-/\varepsilon} = C^2, \\ C_{\mathrm{IC}}^R &= e^{-\pi\beta_-/\varepsilon}(1 - e^{-\pi\beta_-/\varepsilon}) = C(1-C), \end{aligned} \tag{31}$$

where the meaning of the coefficients are illustrated in Fig. 3. For a magnetosonic wave incident from above we find that

$$\begin{aligned} T_{\mathrm{MS}} &= e^{-\pi\beta_-/\varepsilon} = C, \\ R_{\mathrm{MS}} &= (1 - e^{-\pi\beta_-/\varepsilon})^2 = (1-C)^2, \\ C_{\mathrm{MS}}^R &= e^{-\pi\beta_-/\varepsilon}(1 - e^{-\pi\beta_-/\varepsilon}) = C(1-C). \end{aligned} \tag{32}$$

This process is illustrated in Fig. 4.

In the case of large gap, wave propagation is entirely determined by the interaction at the crossover frequency which, as we have just shown, is characterized by the coefficient $C = e^{-\pi\beta_-/\varepsilon}$. These results can be understood as a series of two mode couplings.[17] A downgoing ion-cyclotron wave with unit flux encounters the crossover frequency at which point a fraction, C, is transferred from branch II to branch I. A fraction, $1-C$, continues down along mode II and is the coupled transmission coefficient C_{IC}^T. The wave which couples to branch I reflects at the cutoff frequency and once again encounters the crossover frequency as an upgoing

Downloaded 21 Jan 2009 to 198.35.0.41. Redistribution subject to AIP license or copyright; see http://pop.aip.org/pop/copyright.jsp

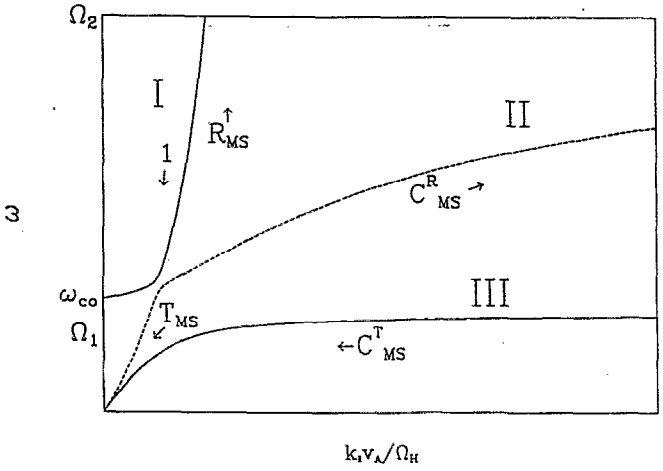

FIG. 4. Illustration of the meaning of the coefficients for a downgoing magnetosonic wave.

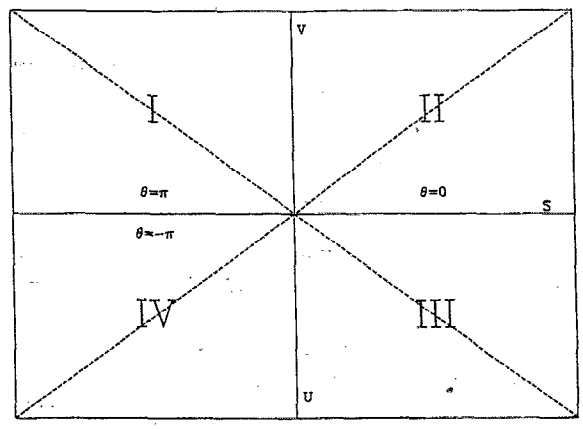

FIG. 5. Sectors of the complex plane divided according to regions of dominance and subdominance of the asymptotic WKB solutions. The Stokes lines and anti-Stokes lines are solid and dashed, respectively.

wave. This reflected wave has amplitude C. Upon coupling, a fraction, C, of this reflected wave flux is coupled to branch II comprising the reflection coefficient $R_{IC}=C^2$. The fraction, $1-C$, remains on branch I and is the coupled reflected wave $C^R_{IC} = C(1-C)$. Although in the limit of a small "gap" the transmission coefficient T_{IC} is a Budden tunneling term, in the limit of a large "gap" T_{IC} vanishes. This analysis differs from previous work[17] in that four propagating asymptotic modes rather than two are involved in the analysis. A similar interpretation may be given to the case of an incident magnetosonic wave as illustrated in Fig. 4.

D. Large κ—Two propagating modes

1. Phase integral analysis

For large enough κ, $\sigma<\kappa^2$, so that two of the solutions of Eq. (21) are complex (n_+ is real and n_- is imaginary). Because two of the asymptotic solutions are growing along the real axis the positive and negative real axes are Stokes lines for two of the solutions while the positive and negative imaginary axes remain the Stokes lines for the other two solutions. The anti-Stokes lines are along the rays $n^0_+x=\pm n^0_-y$ where $z=x+iy$ is the complex coordinate. In order to incorporate the Stokes phenomena we introduce the Stokes multipliers such that upon crossing a Stokes line on which a WKB solution is maximally subdominant the coefficient of that term equals the coefficient before crossing the Stokes lines $+\Sigma_j S_j \times$ the coefficients of the jth dominant term on the Stokes line.[8,25,26]

Appropriate boundary conditions require that at $\pm\infty$ the exponentially growing modes be absent. In addition, appropriate boundary conditions require that no upgoing wave be found at $-\infty$. In order to satisfy these conditions, we assume along or above the positive real axis that the solution takes the form

$$\psi=A\Theta^-_+ + B\Theta^-_- + C\Theta^+_- + D\Theta^+_+ \quad \text{(region II)}. \tag{33}$$

Using the rules stated above we may continue the solution into the following sectors illustrated in Fig. 5,

$$\psi=A\Theta^-_+ + B\Theta^-_- + C'\Theta^+_- + D\Theta^+_+ \quad \text{(region III)}, \tag{34}$$

with $C'=C-AS_1-BS_2-DS_4$

$$\psi=A'\Theta^-_+ + B\Theta^-_- + C'\Theta^+_- + D\Theta^+_+ \quad \text{(region IV)}, \tag{35}$$

with $A'=A-BU_2-C'U_3-DU_4$ and

$$\psi=A\Theta^-_+ + B\Theta^-_- + C\Theta^+_- + D'\Theta^+_+ \quad \text{(region I)}, \tag{36}$$

with $D'=D+AV_1+BV_2+CV_3$ where S, U, and V are Stokes constants. In order to satisfy the boundary conditions for downgoing waves, we require that $B=C=D'=0$, $A=1$. The transmission and reflection coefficients are

$$T_{IC}=\frac{|\Theta^-_+|^2_{\mathrm{Arg}(z)=\pi}}{|\Theta^-_+|^2_{\mathrm{Arg}(z)=0}}=e^{-\pi\beta_+/\varepsilon}, \tag{37}$$

$$R_{IC}=|V_1|^2|\Theta^+_+|^2_{\mathrm{Arg}(z)=0}/|\Theta^-_+|^2_{\mathrm{Arg}(z)=0}=|V_1|^2. \tag{38}$$

In order to determine the Stokes constant V_1 we consider the situation with $B=C=D=0$, $A=1$ from which we can compute the Stokes constant if we invoke the conservation law. On the real axis, the exponentially growing solutions do not contribute to the Poynting flux so that the conserved quantity J/n_+ is

$$J/n_+=\begin{cases} 1, & \mathrm{Arg}(z)=0, \\ e^{\pi\beta_+/\varepsilon}, & \mathrm{Arg}(z)=-\pi, \\ e^{-\pi\beta_+/\varepsilon}-|V_1|^2e^{\pi\beta_+/\varepsilon}, & \mathrm{Arg}(z)=\pi. \end{cases} \tag{39}$$

From the energy discontinuity

$$-\Delta=1-e^{\pi\beta_+/\varepsilon}=-1+e^{-\pi\beta_+/\varepsilon}-|V_1|^2e^{\pi\beta_+/\varepsilon} \tag{40}$$

we obtain the reflection coefficient

$$R_{IC}=|V_1|^2=(1-T_{IC})^2. \tag{41}$$

2. Saddle-point analysis

For large values of κ, the saddle point associated with the crossover frequency is located far from the real axis so that it does not contribute to the coupling process as evidenced by the weak dependence of β_+ on the crossover frequency. Therefore, the saddle point is associated with zero

Downloaded 21 Jan 2009 to 198.35.0.41. Redistribution subject to AIP license or copyright; see http://pop.aip.org/pop/copyright.jsp

frequency at small κ and the oxygen resonance for large values of κ and is of primary interest (see Fig. 2). The transition from four propagating modes to two propagating modes occurs at a critical value of κ. Assuming that r and l take a simple form such as in Eq. (17), the cutoff condition (9) implies that

$$z_{co}=a1-\kappa^2/4k_r^2/(1-\sigma\kappa^2/k_r^2k_l^2). \tag{42}$$

We then find that the abrupt change in the behavior of the modes occurs at the critical value, $\kappa^2=k_r^2k_l^2/\sigma$. For smaller κ, the mode-conversion processes are determined primarily from the saddle point associated with the crossover frequency. For intermediate values of κ, $k_r^2k_l^2/\sigma<\kappa^2<2k_r$, four modes propagate in the vicinity of the heavy ion resonance although the magnetosonic branch is cut off at some point below the gyrofrequency and does not propagate above the gyrofrequency. The dominant saddle point is the one that is associated with zero frequency at small κ and the oxygen resonance at large κ. For larger κ, $\kappa^2>2k_r$, the downgoing ion-cyclotron wave is cutoff above the oxygen resonance at a frequency which approaches the ion–ion hybrid frequency and only two modes propagate. The transmission properties may be obtained by expanding about the saddle point associated with the cutoff condition $rl-\kappa^2s=0$. In the ensuing analysis we follow the reasoning of Lashmore-Davies *et al.*[17] and Fuchs *et al.*,[18,21] and consider the cases of intermediate and large κ separately.

The expression for the location of the saddle point in the complex plane is given by Eq. (11) with the potential (14). The roots of the saddle point occur in complex conjugate pairs so that the potential has the form of a complex conjugate barrier described by the Weber equation. Assuming the form of r and l in Eq. (17), the potential is

$$Q(\xi)=\frac{\delta^2+\kappa^4/4}{4\xi^2(s-\kappa^2/2)}[(\xi-\xi_r)^2+\xi_i^2], \tag{43}$$

where $\xi=\xi_r\pm\xi_i=(k_l^2a/2)(\delta\pm i\kappa^2/2)/(\delta^2+\kappa^4/4)$ is the location of the complex conjugate roots. If we then make the judicious choice for the variables $k_0^2=(\delta^2+\kappa^4/4)/[\xi_r^2(s_r-\kappa^2/2)]$ and $\beta=\xi_i/2=(k_l^2a/2)(\kappa^2/4)/(\delta^2+\kappa^4/4)$ then the embedded equation is a Weber equation which has the transmission coefficient[17,18]

$$T=e^{-2\pi k_0\beta^2/\varepsilon}, \tag{44}$$

where the argument of the exponential is

$$k_0\beta^2=\frac{k_l^2a}{8}\frac{\kappa^4/4\delta}{\sqrt{(\delta^2+\kappa^4/4)(\kappa^4/4\delta+\kappa^2/2-k_r^2)}}. \tag{45}$$

Near the upper limit of validity, the two results have a reasonably simple limit. For $\kappa^2/2=k_r^2$, $\beta_+=(k_l^2a/2)/(\sqrt{\delta^2+k_r^4})$, whereas the equivalent coefficient from the saddle point is $2k_0\beta^2=\beta_+k_r^2/2\sqrt{\delta}$. Over the range of densities for which absorption is strong (0.5%–5%), the ratio, $k_r^2/2\sqrt{\delta}$ takes values ranging from 1.3 to 0.6 depending on the density ratio and the two results are in reasonable agreement.

The form of the reflection coefficient may be understood physically in the same manner that we understood coupling

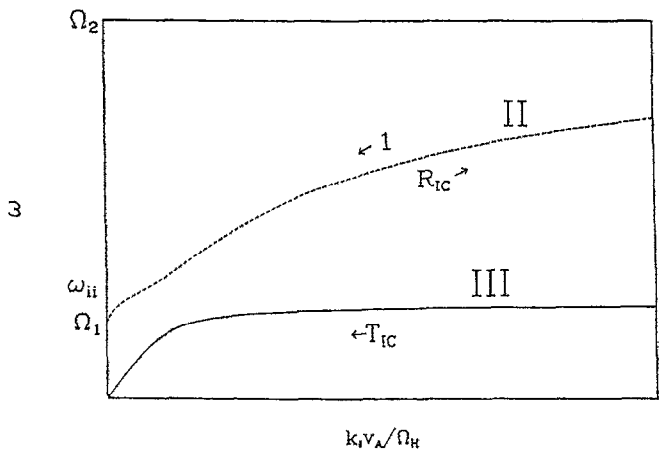

FIG. 6. Illustration of the physical meaning of the coefficients for a downgoing ion-cyclotron wave for large angle of propagation.

for smaller κ. In this case, coupling between the modes is characterized by As illustrated in Fig. 6, incident waves along mode II $T_{IC}=T=e^{-\pi\beta_+}$ and the coefficients may be obtained as a series of two mode couplings.[17]

For larger values of κ we expand about the cutoff-resonance pair which arises near the ion–ion hybrid frequency. The coupling potential in (6) is

$$Q=(rl-\kappa^2s)/(r+l-\kappa^2). \tag{46}$$

After suitable definitions and algebraic manipulation,[8,25] the potential is found to take the Budden form $Q=k_0^2(1-\alpha/z)$. The transmission coefficients are well known

$$T=e^{-\pi k_0\alpha/\varepsilon},\quad R=(1-T)^2. \tag{47}$$

In the limit of large κ the potential approaches

$$Q\approx s=-\frac{\Omega_{c1}^2\Omega_{c2}^2}{\omega_{ii}^2}\frac{(\omega^2-\omega_{ii}^2)}{(\omega^2-\Omega_{c1}^2)(\omega^2-\Omega_{c2}^2)}, \tag{48}$$

which exhibits a cutoff at the ion–ion hybrid frequency and a resonance at the oxygen gyrofrequency. Expanding s about the gyrofrequency, $s\approx\sigma(1-k_l^2a/2\sigma z)$ we find that the coefficient factor is $k_0\alpha=\beta_+=k_l^2a/2\sqrt{\sigma}$ in agreement with (29) of the previous section.

Comparing both this result and the result for intermediate κ, we find that both coefficients are of the Budden form with transmission and reflection coefficients given by T and $(1-T)^2$, respectively. These results compare well with the form (37) and (41) which we obtained using the phase-integral analysis. In this analysis, we have three parameters: k_r, k_l, and a. These three parameters are sufficient to retain the location of the resonance (Ω_{c1}), crossover frequency (ω_{cr}), cutoff frequency (ω_{co}), and ion–ion hybrid frequency (ω_{ii}). Thus, in some sense we can form a uniform approximation which retains the characteristics of the crossover and cutoff frequencies for small κ but retains the characteristics of the ion–ion hybrid resonance for perpendicular propagation. This linear approximation is good if the coupling is dominated by one or the other of the two coupling points, but if both coupling points are of significant importance, one

Downloaded 21 Jan 2009 to 198.35.0.41. Redistribution subject to AIP license or copyright; see http://pop.aip.org/pop/copyright.jsp

suspects that the linear approximation will fail for the phase-integral approach, and Eq. (1) should be solved numerically.

IV. NUMERICAL CONSIDERATIONS

A. Basic equations

In this section we solve Eq. (1) numerically. To proceed, we specify the dependence of the Stix functions (2) on position, z. For simplicity, we take the density to be constant and let the magnetic field vary as for a dipole field, $\Omega_{c1}(z)/\omega \approx L_B^3/x^3 = 1/z^3$ where x is the physical coordinate. The differential equation has a regular singular point at the location of the plasma resonance, namely where $z=1$. The solution to the differential Eq. (1) is multivalued and has a branch point at $z=0$. In order to retain the appropriate physical behavior, we continue the solution above the pole in the complex plane.[4] We refer the reader to a separate report[9] which contains the details and addresses the complications involved in these numerical calculations.

B. Parameter regime

In the following sections we determine the coefficients for several cases of incidence as described previously. The parameters of greatest interest are the magnetic field, magnetic field scale length, and the masses and densities of the various constituent ions. The masses are fixed parameters which we take to be hydrogen and oxygen (both singly ionized). The magnetic field and densities are embedded in the WKB parameter ε and the functions r and l depend only upon the density ratios. Hence, a particular solution is determined from the specification of ε and the concentration of the minority species η. Typical values for the parameter ε are

$$\varepsilon = \frac{1}{k_A L_B} \approx 0.5 r^{-1} \rho^{-1}, \tag{49}$$

where r is the scale length in earth radii ($\sim$1–3) and ρ is the number density of ions ($\sim$1–100 cm^{-3}).[27] We explore the parameter space for ε ranging from approximately 0.2 to 0.03. In this range, the WKB approximation is good and provides reasonable matching conditions to the WKB solutions. We concentrate on that range of oxygen concentration consistent with reasonable absorption levels. We have found this range to vary from 0.5% to 5%. In order to consider the limiting case of a large "gap" we take ε to be small and η to be large.

C. Incident magnetosonic waves

For the results of this section, we impose the boundary conditions for downcoming magnetosonic waves as illustrated in Fig. 4. In that figure a wave is incident on the magnetosonic branch with unit flux. The fractions of wave flux $T_{\rm MS}$ and $R_{\rm MS}$ are transmitted and reflected on the magnetosonic branch while the fractions $C_{\rm MS}^R$ and $C_{\rm MS}^T$ are transmitted and reflected along the ion-cyclotron branches as indicated.

We have obtained full analytical solutions for the limit of a large "gap." In Fig. 7 we show the numerical solutions to the differential equation. Superimposed on the graph we

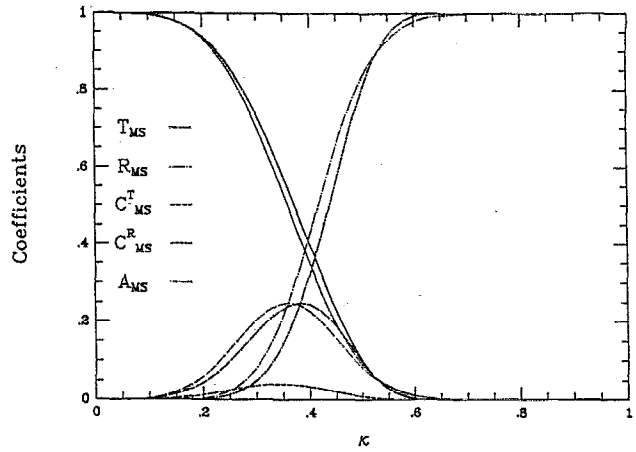

FIG. 7. Coefficients for the limit of a large "gap." The numerical solutions are plotted in bold type and the analytical results are indicated in light type.

have shown the analytical results (32) which we have obtained from a phase integral analysis consistent with a large "gap" for which there is no absorption. The results are in very good agreement. The most striking difference is that the coefficient $C_{\rm MS}^T$ is nonzero in contrast to the analytic situation. However, the analytical results only incorporate the existence of the coupling point near the crossover frequency. Coupling between the two Alfvén waves can be very strong at frequencies below the heavy ion-cyclotron frequency. It is this coupling which gives rise to the wave power found on the ion cyclotron branch.

Even in the limit of a small "gap," the analytical results are in reasonable agreement. In Fig. 8 we have plotted the coefficients for the case $\varepsilon=0.2$ and $\eta=1\%$. For parallel propagation, no coupling occurs. As κ increases, strong coupling between the two transmitted Alfvén waves occurs, and the sum of those coefficients reproduces the analytical transmission coefficient. This coupling is a result of the presence of both saddle points. For large κ waves are reflected in the two upward propagating modes. The cutoff frequency increases substantially for large enough κ and the "gap" becomes too large to penetrate. In this case the reflection coef-

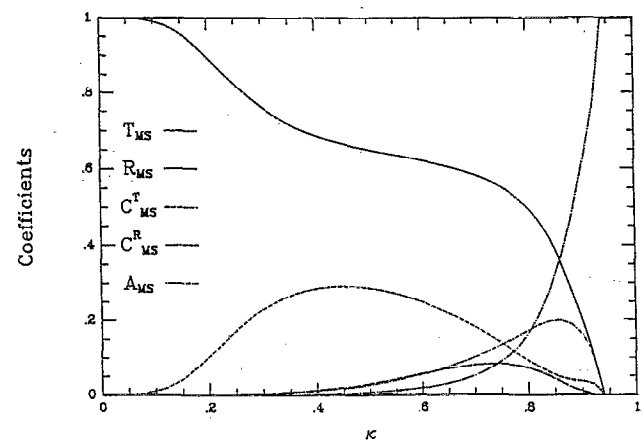

FIG. 8. Coefficients for the case $\varepsilon=0.2$ and $\eta=1\%$.

Downloaded 21 Jan 2009 to 198.35.0.41. Redistribution subject to AIP license or copyright; see http://pop.aip.org/pop/copyright.jsp

ficient grows rapidly, and for $\kappa \approx 0.95$ the magnetosonic wave no longer propagates (the wave is reflected at the lower-hybrid frequency well above the hydrogen gyrofrequency). For a substantial range of κ strong absorption occurs peaking at 20% for large κ.

For smaller densities, the absorption increases to about 25% although it tends to sharpen and occur mostly at large κ. As the minority species density tends to zero, the transmission coefficient, T_{MS}, is approximately 1 and all other coefficients vanish. This means, in effect, that for very small oxygen densities the waves propagate as if there were no oxygen present.

For larger densities (η=5%) we find that the absorption diminishes rapidly although the waves still couple at low altitude. In addition, we find that total reflection occurs at a much smaller value for κ. Absorption appears to be very small. However, one should keep in mind that in the case of a large gap all power upcoming in the LHCP mode will be absorbed. If perfect reflection were to occur at ionospheric altitudes, it is conceivable that a substantial portion of C^T_{MS} would also be absorbed.

For smaller values of ε (=0.08) we find that less coupling occurs between the two downgoing transmitted waves. In addition, reflection is much stronger at intermediate values of κ. This is because the "gap" contains more wavelengths and transmission is substantially diminished. Reasonably strong absorption still occurs over a vast range of κ and is typically about 7%. It should also be noted that a substantial portion of the reflected wave C^T_{MS} can also contribute to heating upon reflection. For even smaller values of the parameter ε (=0.03) we find that the absorption becomes negligible for $\eta > 1\%$, however, the absorption remains reasonably significant for $\eta = 0.5\%$.

In summary, we have found that incident magnetosonic waves couple strongly near the crossover frequency for reasonable values of the minority species density. For larger values of κ the waves are completely reflected, and strong absorption occurs over a substantial range of κ.

D. Incident ion-cyclotron waves

For the results of this section, we impose the boundary conditions for downcoming ion-cyclotron waves. For values of κ smaller than the critical κ for which the magnetosonic mode is cut off we determine these values numerically. For larger values of κ we use the analytical results obtained earlier. In this section we obtain correct estimates of the absorption for both small and large values of κ, and we will discuss the meaning and correctness of evaluating the coefficients for intermediate κ.

First consider the coefficients for values of κ smaller than the critical κ for which the magnetosonic mode is cut off as illustrated in Fig. 3. A wave is incident on the ion-cyclotron branch with unit flux. The fractions of wave flux T_{IC} and R_{IC} are transmitted and reflected on the ion-cyclotron branches while the fractions C^R_{IC} and C^T_{IC} are transmitted and reflected along the magnetosonic branch as indicated.

We have obtained full analytical solutions for the limit of a large "gap." In Fig. 9 we show the numerical solutions to the differential equation. Superimposed on the graph we have shown the analytical results (31) which we have obtained from a phase-integral analysis consistent with a large "gap" for which there is no absorption. As for the case of an incident magnetosonic wave, the results are in very good agreement. Again a small amount of wave flux is found in the coupled transmitted wave.

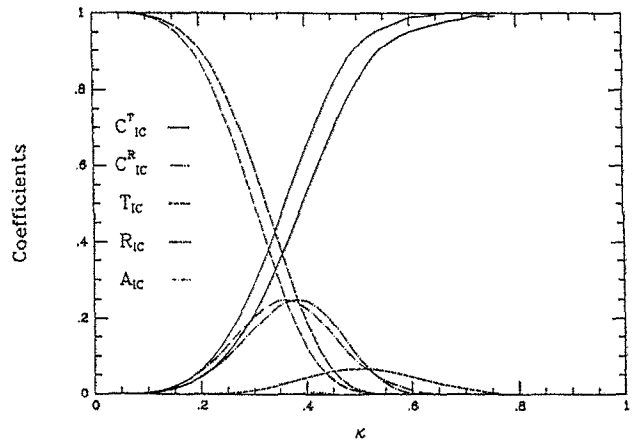

FIG. 9. Coefficients for the limit of large "gap."

In Fig. 10 we have plotted the coefficients for a small "gap" with ε=0.2 and η=1%. For parallel propagation, the problem is describable as a Budden tunneling problem for the ion-cyclotron branch, and the ion-cyclotron and magnetosonic branches do not couple. For small values of κ the low frequency coupling point does not enter into the calculation so the analytical analysis is quite accurate. As κ increases, coupling between the downgoing modes occurs at the crossover frequency, and substantial wave energy is transferred to the coupled magnetosonic waves. The existence of two *different* coupling points (low frequency and crossover—see Fig. 2) also leads to coupling between the transmitted and coupled transmitted modes. Substantial absorption occurs over a very large range of κ taking a value over 20% over most of the range. In Fig. 11 we explore the

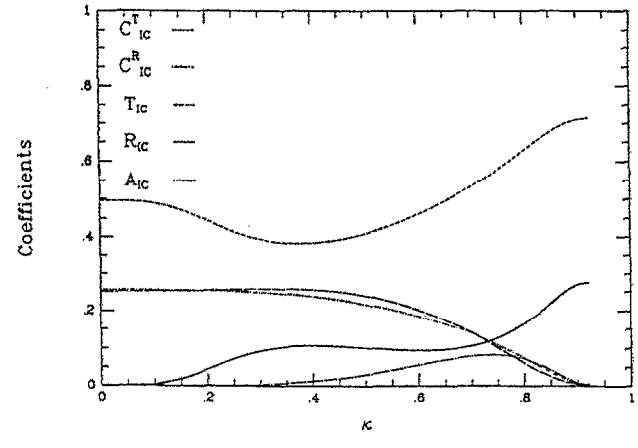

FIG. 10. Coefficients for the case ε=0.2 and η=1%.

Downloaded 21 Jan 2009 to 198.35.0.41. Redistribution subject to AIP license or copyright; see http://pop.aip.org/pop/copyright.jsp

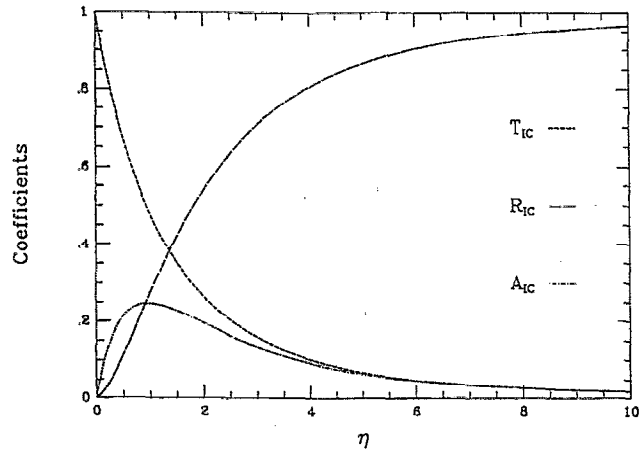

FIG. 11. Coefficients for parallel propagation with $\varepsilon=0.2$.

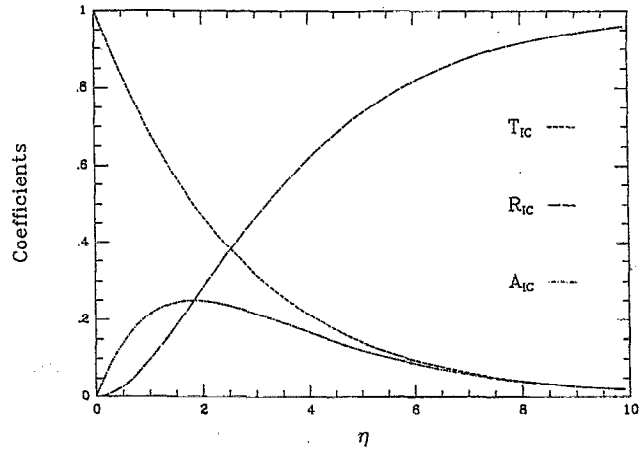

FIG. 13. Coefficients for large κ with $\varepsilon=0.2$. Strong absorption occurs for $0.5<\eta<5$.

transmission coefficients for parallel propagation for $\varepsilon=0.2$ (for parallel propagation the two modes are uncoupled so that $C_{IC}^R = C_{IC}^T = 0$). As is clear, substantial absorption occurs over a large range of densities ranging from $\eta=0.5\%$ to $\eta=4\%$. For larger values of κ, the absorption remains essentially the same as for parallel propagation up to reasonably large values of κ.

For large values of κ, we have shown using a variety of methods that the transmission properties are described as a Budden tunneling problem at the ion–ion hybrid frequency. In Fig. 12 we have plotted in bold type the transmission factors found in Eqs. (37) and (41) along with the corresponding absorption factor. Physically, the coefficients correspond to Fig. 6. In light type we have plotted the transmission factors obtained from the embedded differential equation (47). They are in good agreement in the regime in which they are both valid. It is to be noted that there is reasonable agreement between the transmission factor, T_{IC}, near the upper bound of the numerical solution of Fig. 10 and the large κ solutions of Fig. 12. The absorption and reflection coefficients do not match well. While it is to be expected that the dominant WKB solution would be continuous in κ it is not necessarily expected that the coefficient of the subdominant solutions would remain continuous.

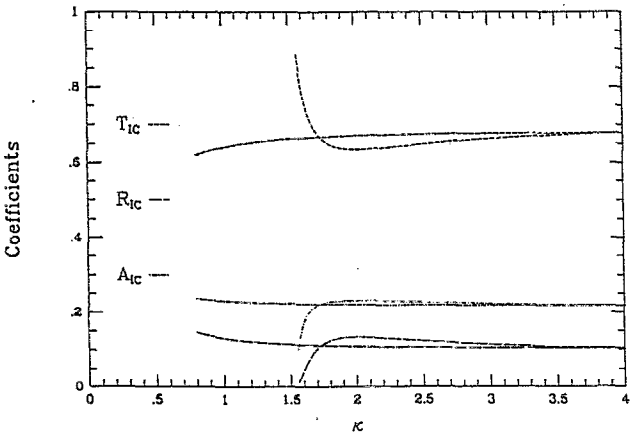

FIG. 12. Analytical approximations for the transmission coefficients for $\varepsilon=0.2$ and $\eta=1\%$ at large κ.

For large κ the transmission coefficients approach a constant value determined from Budden tunneling at the ion–ion hybrid frequency. In Fig. 13 we plot the coefficients against the concentration of oxygen. As for the case of parallel propagation strong absorption occurs for a large range of densities ranging from $\eta=0.5\%$ to $\eta=7\%$. In all cases the absorption remains essentially constant for $\kappa>1$. For smaller values of ε the region of strong absorption moves to smaller values of η.

In summary, we have found that incident ion-cyclotron waves undergo Budden-like tunneling at the cutoff frequency for nearly parallel propagation and at the ion–ion hybrid frequency for nearly perpendicular propagation. The absorption is very strong over a large range of κ and for a reasonable range of η. For intermediate values of κ, coupling near the crossover frequency becomes important and a substantial amount of wave power is transmitted in the magnetosonic mode. However, for large enough κ, the magnetosonic mode is cut off and that wave power is reflected back into the system.

E. Validity of analytic approximation

The analytic results that were obtained in Sec. III and those obtained by Le Quéau and Roux[19] are in excellent agreement for small and large κ for which one or the other of the two saddle points dominate the mode-conversion process. However, for a small "gap" there is substantial coupling between the two downgoing modes resulting from the cutoff saddle point. The numerical results have the advantage of being able to retain both saddle points. It is also important to point out that the absorptions published by Le Quéau and Roux[19] are somewhat misleading. They show strong absorption for $\eta\approx 10\%-50\%$. First, their approximation is only valid for densities less than 3%. Second, our results clearly show that absorption is at best limited to densities below about 5%. The reason behind this discrepancy is that they

Downloaded 21 Jan 2009 to 198.35.0.41. Redistribution subject to AIP license or copyright; see http://pop.aip.org/pop/copyright.jsp

have fixed the ratio of their tunneling factor, $\eta L_B/\lambda$, so that the WKB approximation is actually not valid for η more than about 1%.

V. CONCLUSIONS

This mode-conversion analysis provides confirmation that equatorial waves are a viable source for ion energization along central plasma sheet field lines. In essence, we have shown that should waves reach the mode-conversion layer there can be substantial transmission and absorption. (This consequence is true also of any intermediate ion, such as helium, that might be encountered en route.) We suggested[4] that the bulk of the waves responsible for heating were ion-cyclotron waves generated near the hydrogen or helium gyrofrequency. Typical values for the parameter ε lie between 0.2 and 0.03 along these field lines. The value of the oxygen to hydrogen density ratio is not well known, but a typical value of 5% or less is not unreasonable during a quiescent period. We have examined the absorption for these typical parameters and find that roughly 10%–20% of the incident waves can be absorbed. This finding is consistent with the previous ion-conic theory which supposes that roughly one-eighth of the observed wave power contributes to ion heating. Essentially what we have shown is that waves do have access to the altitudes where the conics are observed and that sufficient wave power can be absorbed to provide the observed ion energization.

Although we have affirmed that power is available to heat the ions if the waves are incident from the equatorial region, we have by no means provided a complete description of the absorption process. The mode structure and conversion coefficients are likely to be affected by thermal effects (although these results should be good for an order of magnitude estimate). Perhaps more importantly, other physical effects such as boundary conditions need to be considered. As an example of the importance of boundary conditions, suppose we were to assume that waves incident on the ionosphere are completely reflected. Then in terms of the phase-integral analysis, we find trivially that for an incident upgoing ion-cyclotron wave from below the ion gyrofrequency the amount of wave flux $T_{\mathrm{IC}}=\exp(-\pi\beta_+/\varepsilon)$ continues upward. Because this mode is completely subdominant, it couples to no other modes and hence, the remaining wave power is completely absorbed. Thus, for example, in if no absorption occurs, we would find that 60%–70% of the flux transmitted on the coupled branch as C^T_{MS} would be reflected at the ionosphere and then absorbed at the oxygen resonance so that in actuality the coefficients which we have obtained serve as a lower bound.

In sum, our results provide insight with regard to a lower bound estimate of the absorption near the resonance–cutoff–crossover frequency triplet. The results will be somewhat modified if we include more physics into our analysis, but it is certainly clear that substantial wave power is available to heat minority species ions such as oxygen.

ACKNOWLEDGMENTS

This work was supported at the Geophysical Institute by the National Science Foundation, Contract No. ATM-91-11509, and NASA Contract No. NAG 5-1504, and at Massachusetts Institute of Technology by NASA Grant Nos. NAG5-2255 and NAGW 1532, Air Force Office of Scientific Research Contract No. F49620-93-1-0287, and Phillips Laboratory Contract No. F19628-91-K-0043.

[1] T. Chang, G. B. Crew, N. Hershkowitz, J. R. Jasperse, J. M. Retterer, and J. D. Winningham, Geophys. Res. Lett. **13**, 636 (1986).

[2] J. M. Retterer, T. Chang, G. B. Crew, J. R. Jasperse, and J. D. Winningham, Phys. Rev. Lett. **59**, 148 (1987).

[3] G. B. Crew and T. Chang, Phys. Fluids **31**, 3425 (1988).

[4] J. R. Johnson, T. Chang, G. B. Crew, and M. Andre, Geophys. Res. Lett. **16**, 1469 (1989).

[5] S. J. Buchsbaum, Phys. Fluids **3**, 418 (1960).

[6] S. J. Buchsbaum, Phys. Rev. Lett. **5**, 495 (1960).

[7] R. L. Smith and N. M. Brice, J. Geophys. Res. **69**, 5029 (1964).

[8] See AIP Document No. PAPS PHPAE-02-1274-58 for 58 pages of Report No. CSR-TR-92-1 by J. R. Johnson, T. Chang, and G. B. Crew, 1994. Order by PAPS number and journal reference from American Institute of Physics, Physics Auxiliary Publication Service, 500 Sunnyside Blvd., Woodbury, New York 11797-2999. The price is $1.50 for each microfiche (60 pages) or $5.00 for photocopies of up to 30 pages, and $0.15 for each additional page over 30 pages. Airmail additional. Make checks payable to the American Institute of Physics.

[9] See AIP Document No. PAPS PHPAE-02-1274-52 for 52 pages of Report No. CSR-TR-92-2 by J. R. Johnson, T. Chang, and G. B. Crew, 1994. Order by PAPS number and journal reference from American Institute of Physics, Physics Auxiliary Publication Service, 500 Sunnyside Blvd., Woodbury, New York 11797-2999. The price is $1.50 for each microfiche (60 pages) or $5.00 for photocopies of up to 30 pages. Airmail additional. Make checks payable to the American Institute of Physics.

[10] D. G. Swanson, Phys. Rev. Lett. **36**, 316 (1976).

[11] J. Jacquinot, B. D. McVey, and J. E. Scharer, Phys. Rev. Lett. **39**, 88 (1977).

[12] F. W. Perkins, Nucl. Fusion **17**, 1197 (1977), and references therein.

[13] K. Försterling, Hochfreq. Elek. **59**, 10 (1942).

[14] T. H. Stix, *The Theory of Plasma Waves* (McGraw-Hill, New York, 1962), Secs. 2.5 and 3.5.

[15] R. B. White, S. Yoshikawa, and C. Oberman, Phys. Fluids **24**, 384 (1982).

[16] R. A. Cairns and C. N. Lashmore-Davies, Phys. Fluids **26**, 1268 (1983).

[17] C. N. Lashmore-Davies, V. Fuchs, and R. A. Cairns, Phys. Fluids **28**, 1791 (1985).

[18] V. Fuchs, A. Bers, and L. Harten, Phys. Fluids **28**, 177 (1985).

[19] D. Le Quéau and A. Roux, J. Geophys. Res. **98**, 14,946 (1992).

[20] K. G. Budden, *The Propagation of Radio Waves* (Cambridge University Press, Cambridge, 1985), 669 pp., Secs. 19.5 and 19.6.

[21] V. Fuchs, K. Ko, and A. Bers, Phys. Fluids **24**, 1251 (1981).

[22] D. G. Swanson, *Plasma Waves* (Academic, San Diego, 1989), Chap. 6.

[23] C. M. Bender and S. A. Orszag, *Advanced Mathematical Methods for Scientists and Engineers* (McGraw-Hill, New York, 1978), 593 pp.

[24] J. Heading, *An Introduction to Phase Integral Methods* (Wiley, Methuen, 1962).

[25] J. R. Johnson, thesis (1992).

[26] J. Heading, Proc. Cambridge Philos. Soc. **53**, 419 (1957).

[27] T. E. Moore, D. L. Gallagher, J. L. Horwitz, and R. H. Comfort, Geophys. Res. Lett. **14**, 1007 (1987), and references therein.

Downloaded 21 Jan 2009 to 198.35.0.41. Redistribution subject to AIP license or copyright; see http://pop.aip.org/pop/copyright.jsp